Int j simul model 21 (2022) 3, 501-512
Original scientific paper

CONTROL OF WELDING RESIDUAL STRESS AND DEFORMATION FOR THE ROD SUPPORT OF A CRANE

Zhou, Q. H.[*,#]; Zhu, X. Y.[*]; Sun, J. M.[*] & Li, J.[**]
[*] School of Mechanical-Electrical and Vehicle Engineering, Beijing University of Civil Engineering and Architecture, Beijing, 100044, China
[**] AVIC Construction Group Co., Ltd., Beijing, 101407, China
E-Mail: zhouqinghui@bucea.edu.cn ([#] Corresponding author)

Abstract
The counter jib and rod support are the main stress-bearing parts of crane due to large load. But the long weld seams of their joints produce great residual stress and deformation affecting the welding strength. In order to reduce the residual stress and the deformation simultaneously, an optimal welding procedure was proposed considering the effective length of welding seam. Firstly, a theoretic model of welding seam was built as T-joint of Q355 steel. The accuracy of model was verified by the welding experiments. By numerical simulation, the appropriate welding process parameters were obtained. Four welding procedures were designed to investigate the influence of the welding sequence. Results show that the welding sequence has a great influence on residual stress and deformation of the long welding seam. The welding quality can be improved by segmented welding and simultaneous welding. The optimized welding procedure of long welding seam can reduce the residual stress by 8.04 % and the maximum deformation by 74.1 % considering welding sequence. Therefore, it is recommended in the actual welding process of crane.
(Received in April 2022, accepted in June 2022. This paper was with the authors 3 weeks for 1 revision.)

Key Words: Tower Crane, Welding, Residual Stress, Numerical Simulation, Deformation

1. INTRODUCTION

Welding is the main connection type of tower cranes. The traditional welding process mainly relies on experience and rarely on welding laws [1], and the deformation and strength of welding seams could be hardly controlled during welding, resulting in an increasing reject rate. Disastrous accidents may occur if the key parts in the metal structures of a tower crane have poor welding quality [2]. Fig. 1 shows the problems of a tower crane at a construction site. The welding seams with a crack are 35 and 65 mm wide.

Figure 1: Problems of welding seams on a tower crane.

In addition, the residual stress generated in the welding process may increase the maintenance cost, and in turn delay the construction period. Even worse, the residual stress may damage the weldment and lead to accidents [3].

With the rapid development of computer technology, the numerical simulation method has played a significant role in predicting welding deformation and residual stress [4]. The

maximum residual stress point can be found by predicting the residual stress through numerical simulation. Then, the maximum residual stress can be reduced by taking measures, like process optimization, to effectively decrease the weldment reject rate. However, the prediction accuracy is affected by many factors (e.g., actual welding conditions and parameters) during the numerical simulation of welding [5, 6].

Low-alloy high-strength structural steel is the dominant material of a flat-top tower crane. The load carried by the connection between the counter jib and the rod support, which are the key metal structural components, is great in Fig. 2. To improve the load-carrying capacity, the weld length is usually increased, resulting in an extremely long welding seam. The extremely long welding seam will in turn lead to a high welding residual stress, causing the "over-welding" phenomenon and increasing the risk of structural deformation or cracking [7].

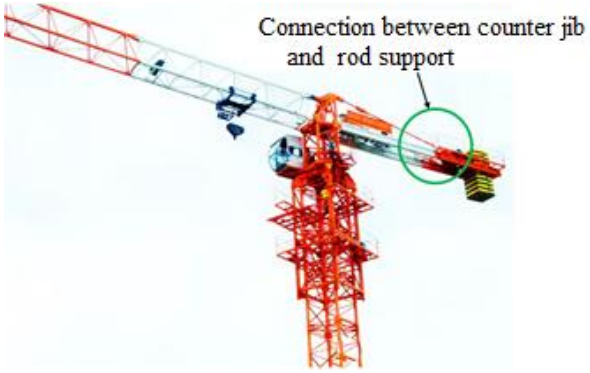

Figure 2: Connection between counter jib and rod support.

Thus, the rod support on the counter jib of a QTZ100 (H6013) flat-top tower crane was taken as the study object. The optimal welding parameters were selected through numerical simulation to explore the influence of the welding sequence on the maximum residual stress and deformation. As a result, the welding quality was improved while ensuring an effective weld length, providing guidance to the lightweight design for flat-top tower cranes.

2. STATE OF THE ART

Welding processes, the welding residual stress distribution, and the numerical simulation of welding have been extensively investigated. Fu et al. [8] studied the welding residual stress of the T-joint and discovered that the stress is concentrated near the start or end point of welding, but not considering the welding process. Romanin et al. [9] proposed a method that could be more easily implemented in universal finite element codes and reported the preliminary result. Their results show that the direction and order of magnitude of deformation are predictable, but the welding sequence could not be optimized. Peng et al. [10] combined the finite element method (FEM) and experimental study to explore the influences of the welding sequence, the welding direction of the cover layer, and the weld reinforcement on the welding effect. However it was only analysed the welding process and not the welding seams. Bai et al. [11] proposed that the welding sequence and direction exert more significant influences on the longitudinal residual stress than on the transverse residual stress. However, the specimens were not studied under actual working conditions. Zhang et al. [12] acquired an accurate simulation result of the experimental residual stress on S355J2 steel based on the bainite transformation, rather than structural parameters. Tankova et al. [13] probed the residual stress field in welded steel members and combined experiment and numerical simulation to predict the residual stress and its distribution in the structure for welded I section, but the I section is different from the T-shape, i.e., the rod support on the counter jib of a tower crane. Wang et al. [14] developed a thermal elastoplastic finite element model to simulate the welding residual stress and the

deformation of low-alloy high-strength steel joints. They explored the influence of the welding sequence on the residual stress distribution and deformation of the butt weld joints of the Q345 H-shaped steel. However, it depends on the section H-shape, also different from T-shape. Liu and Chung [15] experimentally and numerically investigated the residual stress of the S690 H-shaped welding steel, and accurately predicted the residual stress distribution. However, the material of simulation in the welding process is different from Q355, which is the most widely used in tower crane. With the improvement of computer performance and the maturation of finite element (FE) method, numerical simulation has become a very convenient and effective tool to study the residual stress and welding deformation. Kulkarni [16] established a data-driven model via neural network to effectively calculate the residual stress at the welded part and save time. The prediction result was compared with the dataset to determine the accuracy, but a database use for comparation must be constructed for the model. Nishimura et al. [17] obtained more accurate simulation results using the numerical model. They also considered the thermal softening behaviours by verifying the measured data, and used the established model to analyse the influence of the thickness of steel plate on the welding deformation and residual stress of steel overlap joints. However, compared with ultra-high strength steel, Q355 is much more prominent due to lower stiffness. Farrokhi et al. [18] developed a new three-dimensional heat source model for the mixed laser process to simulate full penetration welding and then established a laser welding biconical model, but the whole phenomenon in the process is not yet possible when welding. Deng and Midekazu [19] used the FEM to predict the residual stress distribution in butt-weld steel pipes and considered the metallurgical phase change. Although the calculation result is consistent with the experimental measurement result, their actual working condition has a great difference from construction site. Although finite element welding simulation has been performed on different materials [20-23] and different joint types [24-27], some important welding parameters from structural optimization (e.g., the length of welding seam) and welding process (e.g., welding voltage) were less considered in the numerical simulation process, especially for the welding seam longer than the effective length. Just as this study, the welding seam of the rod support was much longer in the QTZ100 (H6013) flat-top tower crane. To improve the quality of long welding seam, an effective welding way should be found but it is difficult because residual stress and deformation present opposite variation trends to a great extent.

Therefore, to reduce the maximum residual stress and deformation simultaneously, welding experiment and numerical simulation were carried out on a welding specimen. Next, the accuracy of the theoretical model was verified by comparing the specimen experimental deformation with that obtained through numerical simulation. Then, a finite element model of the rod support was established, and appropriate welding process parameters were selected to analyse the influences on the residual stress and deformation. Based on the above processes, the optimized welding control was obtained.

The remainder of this study is arranged as follows. In section 3, the experimental and numerical simulation are described, indicating that the numerical simulation method is accurate and reliable, and the residual stress and deformation of the rod support are theoretically calculated. In section 4, the influences of four welding procedures on the rod support are analysed, and the best welding procedure for the rod support is determined. In the final section, the study is summarized and relevant conclusions are drawn.

3. METHODOLOGY

3.1 Verification analysis of numerical simulation method

General situation of experiment: The base metal was Q355 for which arc welding was adopted, with a voltage of 20 V and a current of 90 A. The dimensions of the flange were the

same as the web with a size of 100 mm × 250 mm × 4 mm. The welding specimen is shown in Fig. 3. The overlapping part between the web and the flange were fixed through successive welding, i.e., the first welding pass was implemented on the right side of the web (the dashed line in arrow). The second pass was performed on the left side (the solid line in arrow).

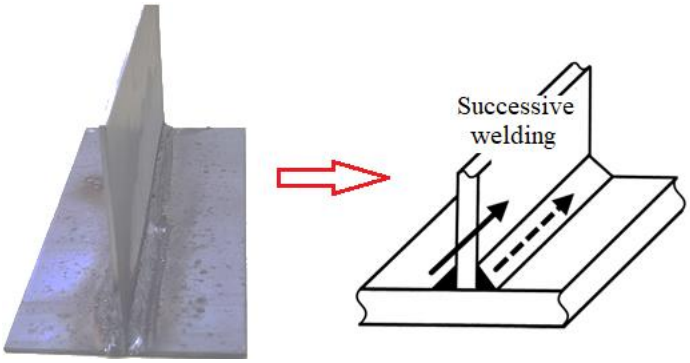

Figure 3: Welding specimen and its welding procedure.

Thermal analysis: A welding heat source model was a mathematical expression of the spatial-temporal thermal input applied on the specimen. The double-ellipsoid heat source models had been widely used to fillet welding and common finite element welding analysis. As shown in Fig. 4.

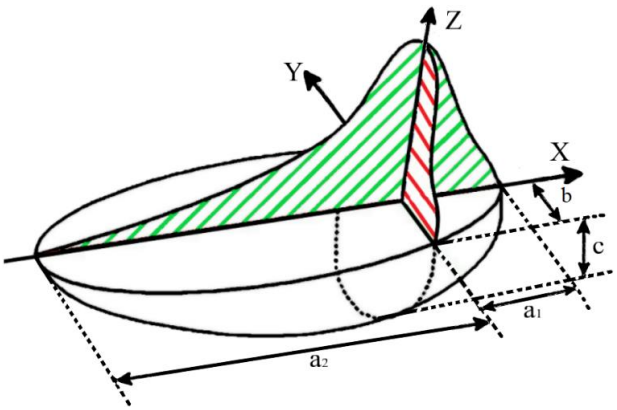

Figure 4: Double-ellipsoid heat source model.

The heat flux distribution of the front half ellipsoid and the rear half ellipsoid can be described as follows:

$$q_1(x,y,z,t)=\frac{6\sqrt{3}f_1q}{\pi^{\frac{3}{2}}a_1bc}\exp\{-3[(\frac{x-vt}{a_1})^2+(\frac{3y}{b})^2+(\frac{3z}{c})^2]\} \tag{1}$$

$$q_2(x,y,z,t)=\frac{6\sqrt{3}f_2q}{\pi^{\frac{3}{2}}a_2bc}\exp\{-3[(\frac{x-vt}{a_2})^2+(\frac{3y}{b})^2+(\frac{3z}{c})^2]\} \tag{2}$$

where $q_1(x, y, z, t)$ and $q_2(x, y, z, t)$ are the power density in the front ellipsoid and in the rear ellipsoid respectively; q is the linear heat input energy, and $q = \eta UI$; U represents the welding voltage; I denotes the welding current; η is the efficiency of the heat source; f_1 represent the portion of the heat deposited in the front ellipsoid, f_2 is the portion of the heat in the rear ellipsoid; and $f_1 + f_2 = 2$; a_1, a_2, b and c are the lengths of the semi-axes.

In case of fillet join, the welding heat input is transferred to the flange and web. The welding parameters determining heat input at the left side were set to be identical with those at the right side. Heats entering web and flange are given as follows [28]:

$$Q_{web} = \frac{t_w}{2t_f + t_w} Q_{total} = \frac{t_w}{2t_f + t_w}(2Q) \tag{3}$$

$$Q_{flange} = \frac{2t_f}{2t_f + t_w} Q_{total} = \frac{2t_f}{2t_f + t_w}(2Q) \tag{4}$$

where Q_{total}, Q_{web}, and Q_{flange} are the total heat, the flange heat, and the web heat, respectively; t_w is the web thickness; t_f is the flange thickness; and Q is the heat input of the left pass or the right pass.

Heat is dissipated to the surrounding environment during the welding. Thus, the convection and radiation between the weldment and the external environment should be considered. The convective heat loss q_c follows the Newton's law as follows:

$$q_c = -h_c(T_s - T_o) \tag{5}$$

where h_c is the heat transfer coefficient, T_s represents the model surface temperature, and T_o is the environment temperature. The heat radiation q_r can be calculated using the Stefane–Boltzmann law.

$$q_r = -\varepsilon\sigma\{(T_s)^4 - (T_o)^4\} \tag{6}$$

where ε denotes the emissivity factor, (0.8); and σ is Stefane–Boltzmann constant (σ= 5.67 × 10^{-8} W/(m^2·K^4)).

Table I: Chemical components of test material.

Material name	C	Mn	Si	P	S	N	Fe
S355J2G3	0.17	1.6	0.02	0.017	0.011	0.005	98.127

Table II: Thermophysical and mechanical properties at different temperatures.

Temperature	T (°C)	20	200	400	600	800	1000	1300	1842
Density	ρ (kg/m^3)	7820	7740	7710	7650	7620	7580	7500	7200
Specific heat capacity	c (J/(kg·K))	460.0	491.7	557.8	667.1	108.0	626.4	637.9	645.5
Heat conductivity coefficient	λ (J/(m·s·K))	50.0	51.1	44.4	39.4	31.8	26.4	29.7	105
Heat transfer coefficient	h_c (J/(m^2·s·K))	1.00	1.50	1.70	1.86	1.98	2.09	2.22	2.29
Yield strength	σ_s (MPa)	380	330	315	280	130	32	20	5
Elasticity modulus	E (GPa)	205	100	150	100	80	19	15	12

Material characteristics: The specimen material was Q355 low-alloy high-strength steel in the Chinese standard (GB/T1591-2018), which corresponds to the S355J2G3 material in the European standard (EN10025-2), and its chemical components and mechanical properties are listed in Table I and Table II. This material contains a small amount of alloying elements. The welding seam filler was set to be the same as the base material.

Verification of model accuracy: The theoretically calculated and experimental deformations are displayed in Fig. 5. Deformation is evident at the two sides of the flange, resulting in angular deformation and the leftward shift of the web. Both the simulation and the experimental results indicate that the welding deformation precents the same variation trends, but the only difference is that the simulation value is slightly smaller than experimental value. The errors of the flange and web are approximately 6.4 % and 6.7 %, respectively. Overall, the numerical simulation results are consistent with the experimental results. The model can correctly reflect the actual welding deformation and the residual stress distribution.

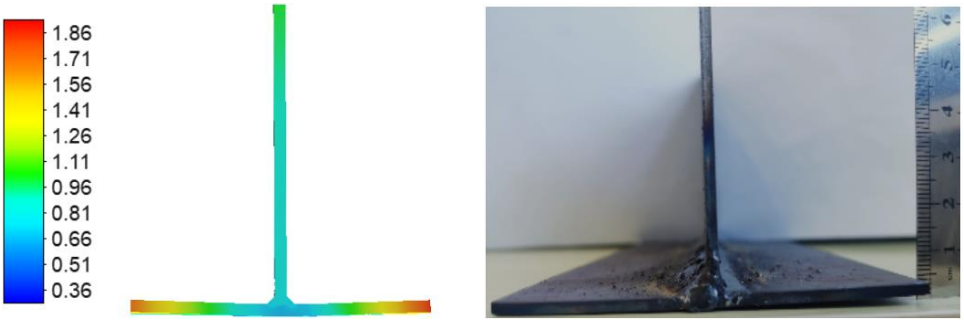

a) Simulation results b) Experimental results

Figure 5: Comparison between simulation results and experimental results.

3.2 Numerical simulation of rod support

Welding parameters for numerical simulation: Welding parameters are important factors influencing the welding quality. During the welding process, the welding effect was impacted by the size and shape of the weld pool, while the width and depth of the weld pool were mainly decided by the voltage and the current. Because the welding current has direct effects on the welding quality and efficiency, it should be as high as possible on the precondition of guaranteeing the welding quality to improve the welding efficiency. However, excessive current could lead to welding seam defects, like undercutting and burning through of the base material. If the current is extremely low, the electric arc will be unstable, thus easily forming welding seam quality flaws, like pores, incomplete penetration, and slag inclusion. The simulated weld pools under six different voltage and current conditions are presented in Table III.

Table III: Six weld pool shapes.

Serial number	**1**	**2**	**3**	**4**	**5**	**6**
Voltage (V)	25	30	30	30	35	30
Current (A)	250	250	300	350	300	350
Weld pool shape	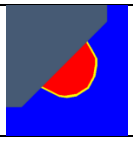	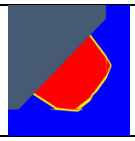	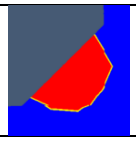	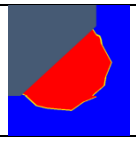	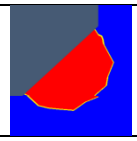	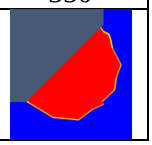

The fist weld pool was very small, which means the welding seam was not completely molten, while the 6th weld pool was too large, meaning the welding seam was excessively molten. The comparison indicates that the shape and size of the weld pool formed by the 4th voltage and current conformed to the actual situation. So, the voltage and current in the simulation was selected to 30 V and 350 A. The welding speed was set to 5 mm/s, and heat source efficiency was 0.8.

Rod support model and its 4 welding procedures: A finite element model of the rod support was established in Fig. 6, with a thickness of 30 mm and a length of 800 mm. The rod support was connected to the counter jib at the bottom through welding.

In order to investigate the influence of the welding sequence on the residual stress and deformation, four welding procedures (A, B, C, and D) were designed in Fig. 7. The arrows represent the welding directions, and the number indicates the welding sequence. Procedure A was successive welding, i.e., number II welding pass was performed after the number I, while procedure B was simultaneous welding on the both sides. In procedure C and procedure D, each welding pass was divided into two or three segments respectively. Segments on the two sides were also simultaneously welded in numerical order.

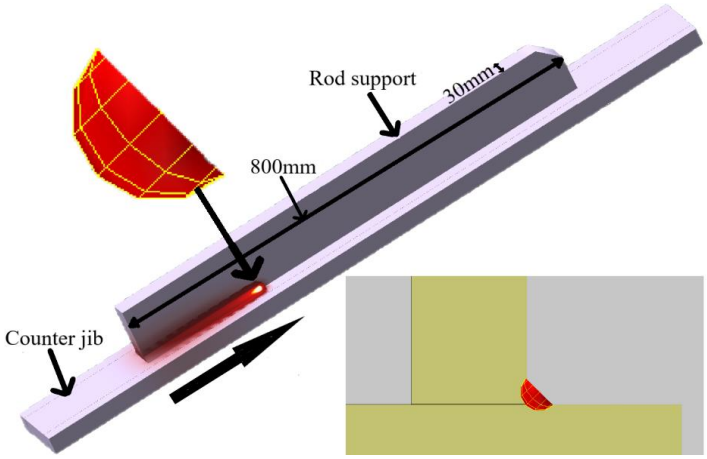

Figure 6: Finite element model of the rod support.

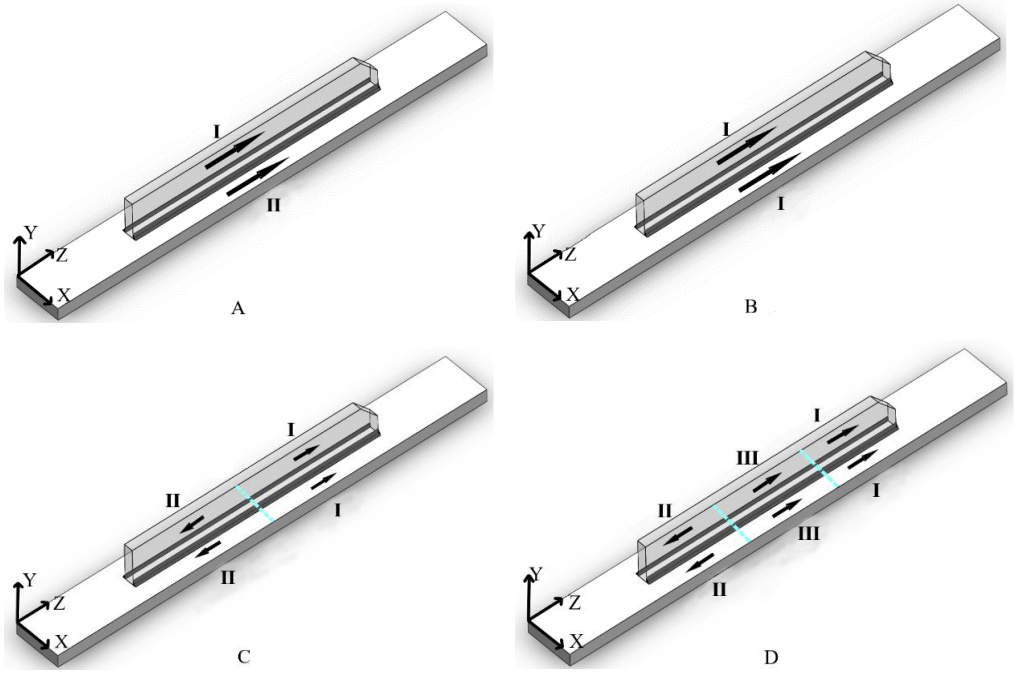

Figure 7: Different welding procedures.

4. RESULT ANALYSIS AND DISCUSSION

4.1 Deformation

The deformations contours in the four procedures are shown in Fig. 8. Compared with procedure A, the maximum deformation in procedure B was reduced by 1.07 mm, i.e., from 2.22 mm to 1.15 mm. However, the maximum deformation in procedure C increased by 0.46 mm and that in procedure D by 0.29 mm.

The deformation in procedure B was the minimum, indicating that the simultaneous welding achieved a smaller deformation than the successive welding. However, if the simultaneous welding was adopted, the segmented welding (Procedure C and Procedure D) would generate a larger deformation than successive welding (Procedure B). The deformation contours in the four procedures (Fig. 8) can also reflect the deformations at different positions. It is obvious that the angular deformation of the flange played a dominant role. The angular deformation was mainly produced by the non-uniform heating when welding. The temperatures of weld areas were high while areas far from the weld were not heated. So, angular deformation occurred due

to different levels of shrinkage and expansion in transvers and longitudinal direction of the structure after cooling.

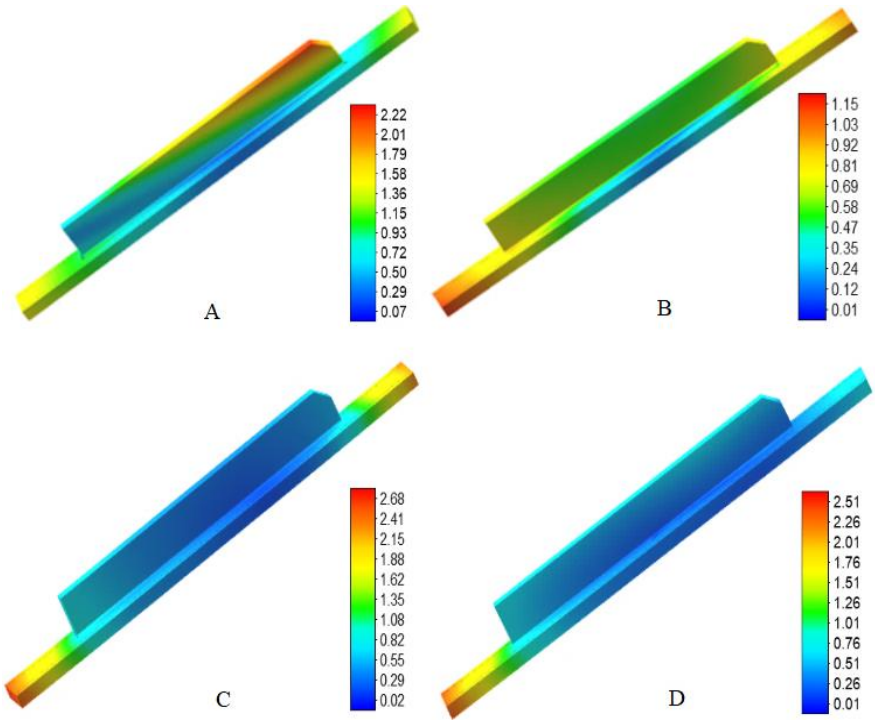

Figure 8: Deformation contours of four procedures.

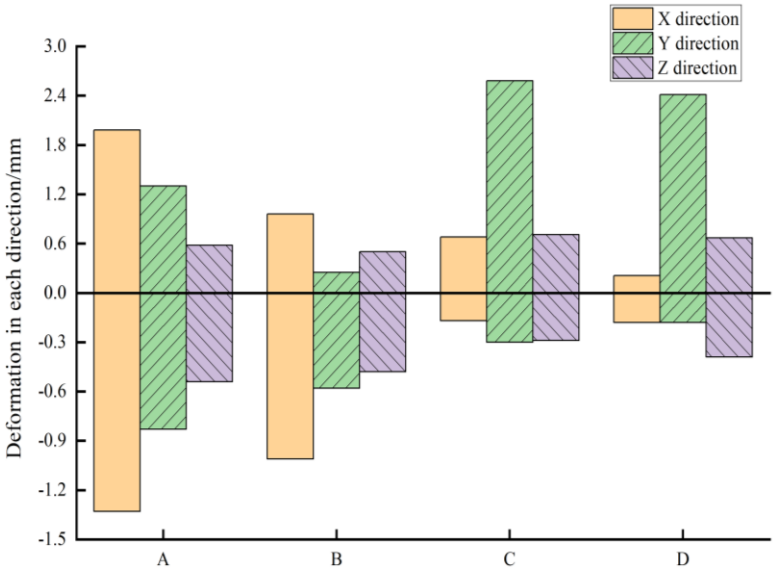

Figure 9: Deformations in different directions in four procedures.

The maximum deformations in the x-y-z directions in the four procedures are also shown in Fig. 9. If the deformation is positive, the deformation is caused by tensile stress. Otherwise, it is generated by compressive stress.

4.2 Residual stress

The residual stress is also influenced by the welding sequence. The simulation of the residual stress in each direction in the four procedures is shown in Fig. 10.

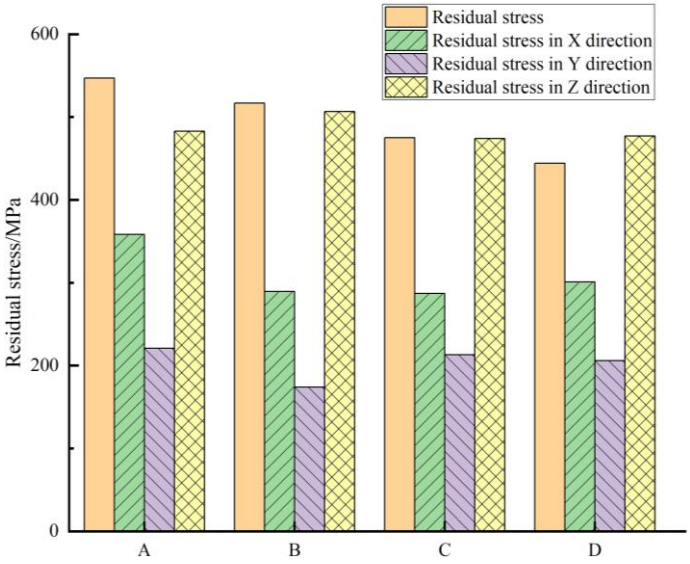

Figure 10: Residual stress in each direction in the four procedures.

Compared with procedure A, procedure B (simultaneous welding) had a minor influence on the longitudinal (z direction) residual stress, but a great influence on the transverse (x direction) residual stress. This phenomenon occurred because during simultaneous welding, the both sides were synchronously heated, the bilateral temperatures were simultaneously raised, and their thermal stresses in the x direction could offset each other, thereby reducing the residual stress. In the case of procedure A (successive welding), the unbalanced thermal stresses in the x direction were maybe generated due to non-simultaneous heat, and the residual stress increased. The transverse residual stress of the weld is directly caused by the transverse shrinkage when cooling. The first welded part cools ahead and restores his internal force balance, which will hinder the transverse contraction of the later cooled part, thus generating higher transverse stress. Therefore, the transverse stress is more sensitive to the welding sequence. The residual stress value in procedure C was smaller which indicates that the peak residual stress of the welding seam can be reduced by welding from the middle to the two ends. In procedure D, the weld pass was performed in three segments which had a good effect on reducing the peak residual stress of the welding seam. It is probably because the segmented welding can reduce the continuous heating time, and the welding temperature is lower leading to the small residual stress.

Briefly, the comparison of residual stress in 4 different procedures indicates that simultaneous welding has a great influence on the transverse (x direction) residual stress. Compared with procedure A, which is adopted in the current production, the transverse residual stress was decreased by 69 MPa in procedure B. Under the condition of simultaneous welding, segmented welding greatly influences the longitudinal residual stress. Compared with procedure B without segmented welding, the longitudinal residual stress was reduced by 33 MPa in the procedure C (2 segments welding), and by 30 MPa in the procedure D (3 segments welding).

4.3 Control for welding residual stress and deformation

The optimal control for welding the rod support was obtained considering the influence of the effective weld length and the welding sequence on the residual stress and deformation. As shown in Fig. 11, the 800 mm long welding seam was divided into 3 segments, each segment in the both ends was 300 mm in length because the effective length of welding seams was 600 mm in the case. And the 200 mm long segment in the middle was free without welding. Simultaneous welding was performed from the middle to the two ends.

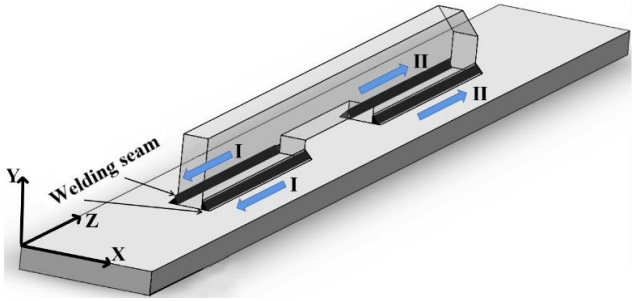

Figure 11: Optimal control for welding.

As shown in Fig. 12, the maximum deformation is only 0.58 mm which is smaller than that in the above 4 welding procedures. To observe the residual stress distribution accurately, 15 tracking points were arranged along the weld toe at an equal distance in Fig. 13. The residual stress value was large in the middle and small at the two ends because the two ends without constraints were free. The simulation results show that compared with procedure A which is the welding process currently used in production workshops, this optimal control can simultaneously reduce the welding residual stress and deformation, where the maximum welding residual stress is reduced by 8.04 % and the maximum deformation by 74.1 %.

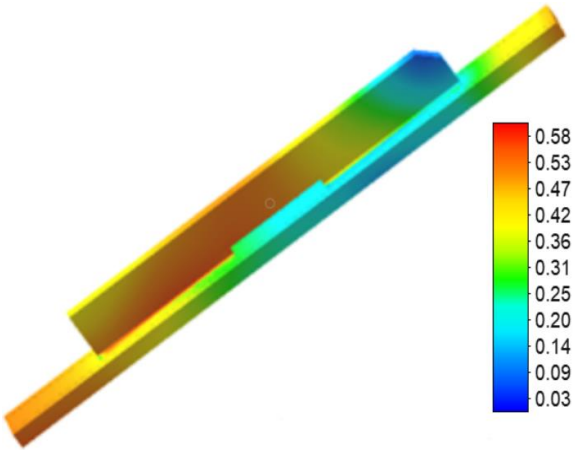

Figure 12: Deformation in the optimal procedure.

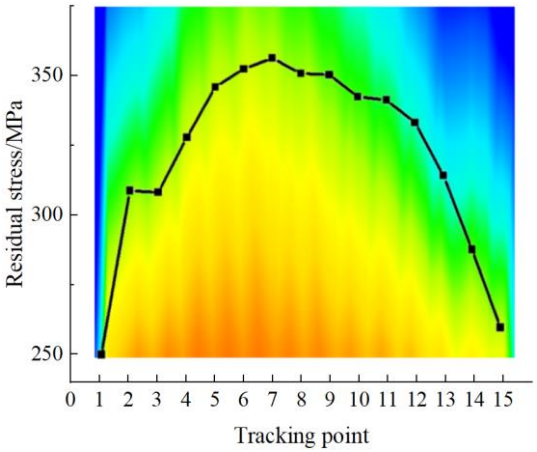

Figure 13: Residual stress with tracking points.

5. CONCLUSION

In general, the welding seams of the rod support in tower cranes are much longer than the effective weld length, causing great residual stress and deformation and increasing the risk of cracking and failure. But it is difficult to solve the problem because the residual stress has an opposite change to the deformation to a great extent. In the study, an optimal welding procedure was proposed to control the welding residual stress and the deformation simultaneously which can provide a guiding significance to the welding production of cranes. The conclusions are drawn as follows:

(1) The numerical simulation is consistent with the experimental result of the welding specimen, proving the accuracy and reliability of the finite element model. Based on the model, the influences of different welding parameters on the welding quality were compared, and the optimal welding parameters were selected.

(2) A reasonable welding sequence is of great importance for improving the welding quality. The simulation indicates that simultaneous welding achieves smaller residual stress and deformation than successive welding. Under the condition of simultaneous welding, the segmented welding reduces the longitudinal residual stress but increases the deformation.

(3) An optimized procedure for welding the rod support was determined considering the influence of the weld length and the welding sequence. Compared with the welding procedure adopted in the current production, the optimized welding procedure can reduce the maximum residual stress by 8.04 % and the maximum deformation by 74.1 %. So, it is recommended in the actual welding process of tower crane.

However, only the dominant material, Q355 low-alloy high-strength steel, was analysed in this study. With the lightweight development of tower cranes, other types of high-strength steel will be widely used, i.e., Q460 should be further discussed on the welding residual stress and deformation considering structural factors in the follow-up studies. And moreover, the intelligent control should be further used in welding sequence to improve welding quality in the actual production.

REFERENCES

[1] Xinyu, H.; Ning, L. (2019). Simulation analysis and prediction of welding deformation of large steel structure frame based on Simufact, *Hot Working Technology*, Vol. 48, No. 21, 147-152, doi:10.14158/j.cnki.1001-3814.2019.21.037

[2] Zrnic, N. D.; Bosnjak, S. M.; Gasic, V. M.; Arsic, M. A.; Petkovic, Z. D. (2011). Failure analysis of the tower crane counterjib, *Procedia Engineering*, Vol. 10, 2238-2243, doi:10.1016/j.proeng.2011.04.370

[3] Rettenmeier, P.; Roos, E.; Weihe, S. (2016). Fatigue analysis of multiaxially loaded crane runway structures including welding residual stress effects, *International Journal of Fatigue*, Vol. 82, Part 2, 179-187, doi:10.1016/j.ijfatigue.2015.04.009

[4] Ghafouri, M.; Ahola, A.; Ahn, J.; Björk, T. (2022). Welding-induced stresses and distortion in high-strength steel T-joints: numerical and experimental study, *Journal of Constructional Steel Research*, Vol. 189, Paper 107088, 17 pages, doi:10.1016/j.jcsr.2021.107088

[5] Dunder, M.; Samardzic, I.; Simunovic, G.; Konjatic, P. (2020). Steel weldability investigation by single and double-pass weld thermal cycle simulation, *International Journal of Simulation Modelling*, Vol. 19, No. 2, 209-218, doi:10.2507/IJSIMM19-2-510

[6] Yang, L.; Yang, B.; Yang, G. W.; Xiao, S. N.; Zhu, T.; Wang, F. (2020). S-N curve and quantitative relationship of single-spot and multi-spot weldings, *International Journal of Simulation Modelling*, Vol. 19, No. 3, 482-493, doi:10.2507/IJSIMM19-3-CO11

[7] Tousignant, K.; Packer, J. A. (2018). Fillet weld effective lengths in CHS X-connections. II: Finite element modelling, parametric study and design, *Journal of Constructional Steel Research*, Vol. 141, 77-90, doi:10.1016/j.jcsr.2017.11.002

[8] Fu, G.; Lourenco, M. I.; Duan, M.; Estefen, S. F. (2016). Influence of the welding sequence on residual stress and distortion of fillet welded structures, *Marine Structures*, Vol. 46, 30-55, doi:10.1016/j.marstruc.2015.12.001

[9] Romanin, L.; Ferro, P.; Berto, F. (2020). Estimation of multi-pass welds deformations with Virtual Weld Bead method, *Procedia Structural Integrity*, Vol. 25, 149-158, doi:10.1016/j.prostr.2020.04.018

[10] Peng, W.; Jiang, W.; Jin, Q.; Wan, Y.; Luo, Y.; Ren, L.; Zhang, K.; Tu, S.-T. (2021). Reduction of welding residual stress in the head-cylinder joint of a large rectifying tower by finite element method and experimental study, *International Journal of Pressure Vessels and Piping*, Vol. 191, Paper 104311, 10 pages, doi:10.1016/J.IJPVP.2021.104311

[11] Bai, R.; Guo, Z.; Tian, C.; Lei, Z.; Yan, C.; Tao, W. (2018). Study on welding sequence of butt-welded structures based on equivalent heat source parameter, *International Journal of Pressure Vessels and Piping*, Vol. 163, 15-22, doi:10.1016/j.ijpvp.2018.04.001

[12] Zhang, K.; Dong, W.; Lu, S. (2021). Finite element and experiment analysis of welding residual stress in S355J2 steel considering the bainite transformation, *Journal of Manufacturing Processes*, Vol. 62, 80-89, doi:10.1016/j.jmapro.2020.12.029

[13] Tankova, T.; da Silva, L. S.; Balakrishnam, M.; Rodrigues, D.; Launert, B.; Pasternak, H.; Tu, T. Y. (2019). Residual stresses in welded I section steel members, *Engineering Structures*, Vol. 197, Paper 109398, 24 pages, doi:10.1016/j.engstruct.2019.109398

[14] Wang, Y.; Feng, G.; Pu, X.; Deng, D. (2021). Influence of welding sequence on residual stress distribution and deformation in Q345 steel H-section butt-welded joint, *Journal of Materials Research and Technology*, Vol. 13, 144-153, doi:10.1016/j.jmrt.2021.04.059
[15] Liu, X.; Chung, K.-F. (2018). Experimental and numerical investigation into temperature histories and residual stress distributions of high strength steel S690 welded H-sections, *Engineering Structures*, Vol. 165, 396-411, doi:10.1016/j.engstruct.2018.03.044
[16] Kulkarni, K. A. (2021). Prediction of welding residual stresses using Artificial Neural Network (ANN), *Materials Today: Proceedings*, Vol. 46, Part 2, 1366-1370, doi:10.1016/J.MATPR.2021.02.486
[17] Nishimura, R.; Ninshu, M.; Liu, Y.; Li, W.; Yasuki, T. (2021). Measurement and analysis of welding deformation and residual stress in CMT welded lap joints of 1180 MPa steel sheets, *Journal of Manufacturing Processes*, Vol. 72, 515-528, doi:10.1016/J.JMAPRO.2021.10.050
[18] Farrokhi, F.; Endelt, B.; Kristiansen, M. (2018). A numerical model for full and partial penetration hybrid laser welding of thick-section steels, *Optics & Laser Technology*, Vol. 111, 671-686, doi:10.1016/j.optlastec.2018.08.059
[19] Deng, D.; Midekazu, M. (2006). Prediction of welding residual stress in multi-pass butt-welded modified 9Cr-1Mo steel pipe considering phase transformation effects, *Computational Materials Science*, Vol. 37, No. 3, 209-219, doi:10.1016/j.commatsci.2005.06.010
[20] Ahn, J.; He, E.; Chen, L.; Pirling, T.; Dear, J. P.; Davies, C. M. (2018). Determination of residual stresses in fibre laser welded AA2024-T3 T-joints by numerical simulation and neutron diffraction, *Materials Science and Engineering: A, Structural Materials: Properties, Microstructure and Processing*, Vol. 712, 685-703, doi:10.1016/j.msea.2017.12.027
[21] Rikken, M.; Pijpers, R.; Slot, H.; Maljaars, J. (2018). A combined experimental and numerical examination of welding residual stresses, *Journal of Materials Processing Technology*, Vol. 261, 98-106, doi:10.1016/j.jmatprotec.2018.06.004
[22] Maksimovic, M.; Maksimovic, K.; Stamenkovic, D.; Vasovic Maksimovic, I. (2021). Initial fatigue life estimation of welded structural components, *Tehnicki vjesnik – Technical Gazette*, Vol. 28, No. 4, 1099-1104, doi:10.17559/TV-20200414015501
[23] Evdokimov, A.; Doynov, N.; Ossenbrink, R.; Obrosov, A.; Weis, S.; Michailov, V. (2020). Thermomechanical laser welding simulation of dissimilar steel-aluminum overlap joints, *International Journal of Mechanical Sciences*, Vol. 190, Paper 106019, 18 pages, doi:10.1016/j.ijmecsci.2020.106019
[24] Dai, P.; Wang, Y.; Li, S.; Lu, S.; Feng, G.; Deng, D. (2020). FEM analysis of residual stress induced by repair welding in SUS304 stainless steel pipe butt-welded joint, *Journal of Manufacturing Processes*, Vol. 58, 975-983, doi:10.1016/j.jmapro.2020.09.006
[25] Ghafouri, M.; Ahn, J.; Mourujrvi, J.; Birk, T.; Larkiola, J. (2020). Finite element simulation of welding distortions in ultra-high strength steel S960 MC including comprehensive thermal and solid-state phase transformation models, *Engineering Structures*, Vol. 219, Paper 110804, 14 pages, doi:10.1016/j.engstruct.2020.110804
[26] Kulawik, A.; Wróbel, J. (2020). Numerical study of stress analysis for the different widths of padding welds, *Strojniski vestnik – Journal of Mechanical Engineering*, Vol. 66, No. 10, 567-580, doi:10.5545/sv-jme.2020.6771
[27] Zhang, Q.-H.; Ma, Y.; Cui, C.; Chai, X.-Y.; Han, S.-H. (2021). Experimental investigation and numerical simulation on welding residual stress of innovative double-side welded rib-to-deck joints of orthotropic steel decks, *Journal of Constructional Steel Research*, Vol. 179, Paper 106544, 16 pages, doi:10.1016/j.jcsr.2021.106544
[28] Liang, W.; Deng, D. (2018). Influences of heat input, welding sequence and external restraint on twisting distortion in an asymmetrical curved stiffened panel, *Advances in Engineering Software*, Vol. 115, 439-451, doi:10.1016/j.advengsoft.2017.11.002